Transparent Long-Pass Filter with Short-Wavelength Scattering Based on *Morpho* Butterfly Nanostructures

Niraj N. Lal,*,[†,§,||] Kevin N. Le,[‡] Andrew F. Thomson,[†] Maureen Brauers,[†] Thomas P. White,[†] and Kylie R. Catchpole[†]

[†]Research School of Engineering and [‡]Department of Physics, Australian National University, Acton, ACT 0200, Australia
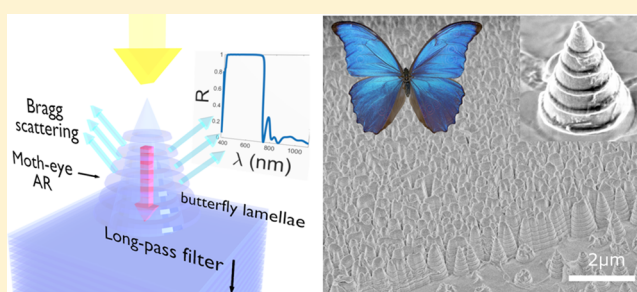[§]Faculty of Engineering, Monash University, Clayton, VIC 3800, Australia
[||]CSIRO Manufacturing Flagship, Clayton, VIC 3168, Australia

S Supporting Information

ABSTRACT: We combine the principles of moth-eye antireflection, Bragg scattering, and thin-film interference to design and fabricate a short-wavelength scattering/long-pass filter with sharp cutoff, high transmission of infrared light, and strong reflection of visible light into high angles. Based on the lamellae-edge features on *Morpho didius* butterfly wings, nanostructures are self-assembled via sequential one-chamber chemical vapor deposition, metal nanoparticle formation, and wet-chemical etching. Finite-element modeling demonstrates strong (>45%) reflection into the first diffracted order for short wavelengths, while retaining >80% transmission for longer wavelengths. Fabricated nanostructures couple more than 50% of reflected light into angles of >10° while enabling broadband long-pass transmission. Such structures have potential applications in light trapping for tandem solar cells, stealth, and signals processing.

KEYWORDS: *Morpho* butterfly, light trapping, tandem solar cell, optical scattering, optical filter

Controlling the transmission and reflection of light from a surface is important for a wide range of technologies including photovoltaics,[1] lighting,[2] stealth,[3] architecture,[4] anticounterfeiting,[5] and signal processing.[6]

Each of these applications has specific optical requirements in terms of scattering direction and intensity, wavelength, bandwidth, and angular dependence. Traditionally, optical components that scatter light are designed to either be highly selective, with a narrow scattering response centered on a particular wavelength,[7] or broadband, with wavelength-independent scattering across the spectrum.[8,9] But for more nuanced applications how can we scatter light? Tandem solar cells, for example, require the selective reflection and scattering of short-wavelength light to a top cell (Figure 1a, d) while ensuring transmission of long wavelengths to an underlying solar cell.[10] Such an optical response is difficult to achieve with either strictly planar or completely irregular surfaces.

We present in this Letter a short-wavelength scattering long-pass filter inspired by *Morpho didius* butterfly wing nanostructures (Figure 1b,c) where we combine the optical principles of moth-eye antireflection, short-wavelength scattering from butterfly wing lamellae, and long-pass transmission from planar dielectric Bragg filters in a single large-area optical component of self-assembled nanostructures (Figure 1d).

Structural color mechanisms inspired by nature have demonstrated a wide range of optical responses including complete broadband absorption,[11] broadband white reflection,[12] metallic reflection,[13] and structural iridescence.[14] Opaque *Morpho* butterfly wing structures have previously been replicated via nanoscale self-assembly,[15,16] achieving strong selective scattering and the striking blue iridescence found on *Morpho* wings. These structures, however, are opaque[17] and selectively scatter light in a narrow range of wavelengths. Broadband response is simple to achieve with planar long- and short-pass optical filters consisting of stacked dielectric multilayers,[18,19] but these afford only specular reflection and transmission.

For tandem solar cells, our initial focus, the condition on angular scattering of reflection is strict:[10] a >2% increase in absolute solar cell efficiency is possible with optimal light trapping, but a sharp decrease in performance is observed with non-wavelength-selective reflection at the interface between top and bottom cells.[10,20−22] Strictly planar reflection is undesirable due to increased out-coupling of light from the top of the cell that could otherwise generate photocurrent in the bottom cell.[10] Three-dimensional inverse-opal photonic crystals are able to provide selective angular reflection, but with nonoptimal transmission in the infrared.[23−25]
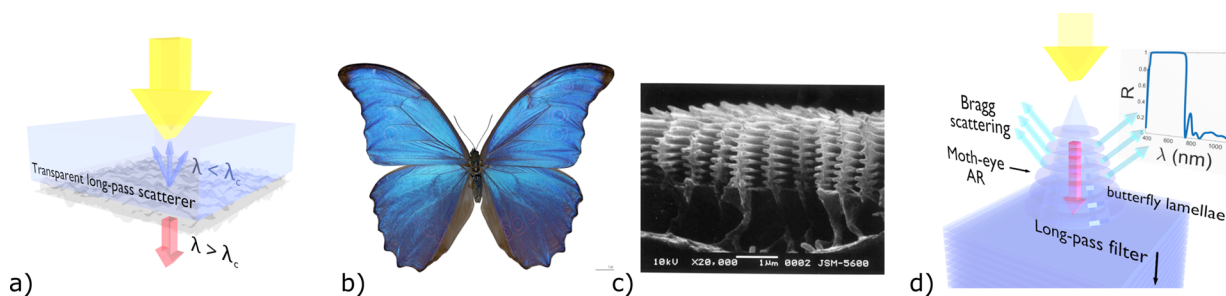
Figure 1. (a) Schematic of a transparent long-pass scatterer with cutoff wavelength λ_c. (b) *Morpho didius* butterfly (male).[41] (c) *Morpho didius* butterfly wing nanostructure SEM [reproduced with permission from *Proc. R. Soc. London B*.[15] (d) Design of transparent long-pass scatterer incorporating moth-eye antireflection, long-pass Bragg filter, and short-wavelength scattering from butterfly wing lamellae.
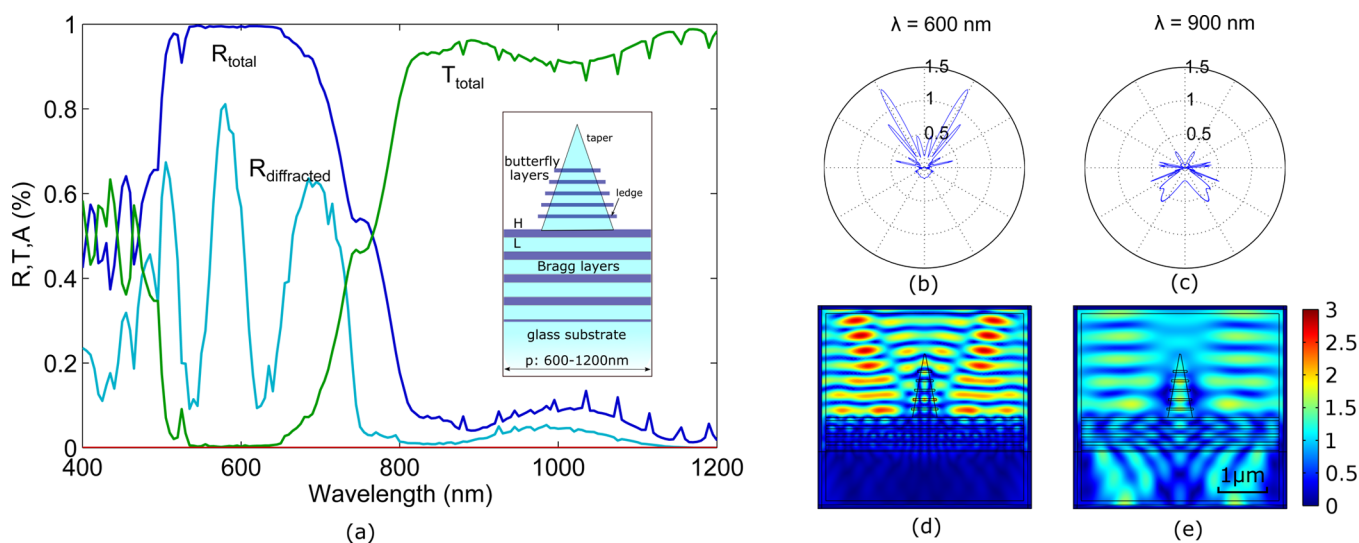

Figure 2. (a) Reflection, transmission, and absorption plots of modeled nanostructures with TiO_2 and SiO_2 high- and low-index layers. (b, c) Polar scattering plots of reflected and transmitted light at 600 and 900 nm, respectively. (d, e) $|E|^2$ intensity profiles at $\lambda = 600$ nm and $\lambda = 900$ nm, respectively.

Motivated by these requirements, we target the three necessary features of a short-wavelength scattering long-pass filter, namely, (1) low long-wavelength reflection; (2) scattering and nonspecular reflection of short wavelengths; and (3) high transmission of long wavelengths.

We achieve them through the combination of various nanostructured elements: moth-eye tapering for antireflection;[26−28] Bragg scattering from butterfly lamellae nanostructures;[16,29−31] and Bragg long-pass transmission from periodic dielectric multilayers.[18,19]

The concept of selective transparency is well established for planar optical elements. We demonstrate here the first selectively transparent optical scattering component by incorporating tapered butterfly lamellae structures *within* the layers of a Bragg long-pass filter, achieving strong forward scattering at narrow angles of long wavelengths and strong backscattering at high angles of short wavelengths.

■ METHODS

Motivated by recent work on perovskite−silicon tandem solar cells where the top cell has a band gap of ∼1.55 eV, we design the structure with a base consisting of a standard Bragg long-pass filter centered on $\lambda_0 = 600$ nm, which enables a reflection/transmission cutoff at the top-cell band gap (∼800 nm). The layer structure is (Air (0.5H) L (HL)^4 Glass),[19] where H and L correspond to quarter-wave layers of the alternating high- and low-index materials, respectively. We first model with ideal high-contrast materials SiO_2 ($n = 1.46$)[32] and TiO_2 ($n = 2.4$)[33] and subsequently with SiO_2 ($n = 1.56$) and SiN_x ($n = 2.12$) layers (collectively labeled SiON), which can be deposited sequentially via plasma-enhanced chemical vapor deposition (PECVD) (see Supporting Information Figure S1).[34] The quarter-wave layers for the initial high and low materials are 62.5 nm (TiO_2) and 102.7 nm (SiO_2) respectively.

The butterfly structure on top of the Bragg filter (inset of Figure 2a) also employs an alternating low−high structure, with layer thickness informed by the structures fabricated by Siddique et al.,[31] at 150 nm for the SiO_2 layer and 40 nm for the TiO_2 layer. The base width of these structures was set to 500 nm, with a ledge width of 50 nm from the structures fabricated by Aryal et al.[16] Four pairs of HL layers were employed in the scattering structure, which had a total height of the structure of 1350 nm, including a final 400 nm thick low index to help elicit the moth-eye antireflection effect for long wavelengths via a gradual refractive-index change.[26] The ledges generate strong Bragg scattering of short-wavelength light as in normal iridescent (though opaque) *M. didius* wing structures,[15] while maintaining the transmission of long-wavelength light (Figure 1d).

We model the structure using two-dimensional (2D) COMSOL finite-element simulations. For reflection and transmission spectra, we use periodic boundary conditions
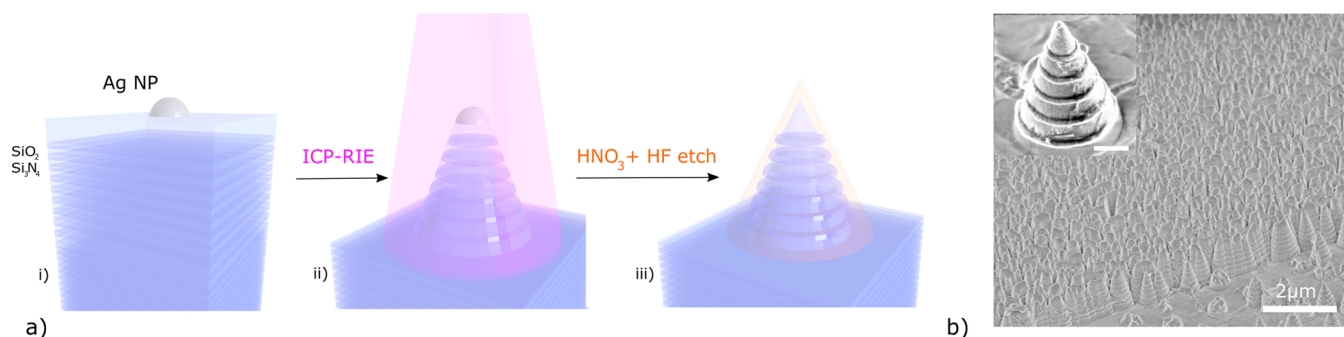
Figure 3. (a) Schematic of nanofabrication self-assembly: (i) PECVD of SiO_2/SiN_x layers with formation of Ag nanoparticles on the surface, (ii) ICP-RIE etching, (iii) chemical wet etch with HNO_3 and then HF. (b) Large-area SEM of nanostructures. Inset: isolated transparent scatterer with a scale bar of 100 nm.

with varying periodicity from 600 to 1200 nm. *E*-field scattering intensity and polar plots for single scattering elements are simulated with perfectly matched layer (PML) boundary conditions with a simulation width of 4 μm to minimize edge effects.

The butterfly structure base width is maintained at 500 nm, with layer thicknesses adjusted for the varying refractive indices. Reflection and transmission spectra are averaged over 20 periods spanning the period range to both simulate the broad power spectrum of periods present in the self-assembled structure[35,36] and to eliminate artifacts arising from the periodic boundary conditions, as discussed further below. Complete modeled data for each individual period are included in Supporting Information Figures S2−S7.

■ RESULTS AND DISCUSSION

In this section we first present numerical modeling results to demonstrate the theoretical feasibility of the approach. We then describe the fabrication process and compare experimental measurements with simulation results.

We first investigate reflection and transmission spectra from a periodic array of scatterers and find excellent, long-pass transmission alongside strong (>95%) short-wavelength reflection, similar to optimized standard Bragg long-pass filters. Spikes in the reflection and transmission spectra are parasitic-reflection artifacts due to linear combinations of Bloch modes within the periodic boundary conditions.[37−39] The strong and broad reflection feature between 450 and 800 nm remains constant across all periods, with the artifacts red-shifting with increasing period (Figures S2−S4). We find high levels of scattering into the first diffracted order (Figure 2a) with strong nonplanar reflection (>45% of reflected light for each period). The tapered scattering structure enhances long-wavelength transmission with strong transmission (>90%) for wavelengths above 800 nm.

The strong nonspecular reflection is directly related to the scattering properties of individual elements. On modeling single scatterers with PML boundary conditions, the polar plot of the time-averaged Poynting vector (with background incident light subtracted) shows the directionality of the scattered and transmitted light at λ = 600 nm (Figure 2b) and λ = 900 nm, respectively (Figure 2c). Field $|E|^2$ intensity profiles demonstrate both strong transmission for long wavelengths (Figure 2e) and scattering of reflected light at short wavelengths (Figure 2d).

Inspired by the modeling, we fabricated structures using SiO_2 and SiN_x layers on microscope glass slides cleaned via

sonication in distilled water, acetone, and 2-propanol for 10 min each. Layers were deposited sequentially via PECVD simply by varying gas composition (T = 400 °C, P = 20 W, pressure = 650 mT, SiN_x: N_2 = 980, NH_3 = 14, SiH_4 = 22 sccm, n = 2.17 (@600 nm), SiO_2: N_2 = 161, N_2O = 710, SiH_4 = 9 sccm, n = 1.515 (@600 nm)), with deposition rates of 2.4 and 8.7 Å/s for high- and low-index layers, respectively. The layer structure is adjusted from the TiO_2/SiO_2 modeled structure with layer thicknesses (Air | Tapered: 400 nm L | Butterfly: (38 nm H, 160 nm L)[5] | Bragg-planar: (69 nm H, 96.2 nm L)[4] | 34.5 nm H | Glass) (Figure S2).

Dielectric layer deposition is followed by metal evaporation of 22 nm of Ag (Angstrom thermal evaporator) and subsequent annealing at 250 °C under N_2 to self-assemble nanoparticles on the surface (Figure 3a,i). These nanoparticles serve as an etch mask for ICP-RIE etching (Figure 3a,ii) (P = 400 W, bias = 60 W, CHF_3 = 50 sccm, He cooling, t = 1000 s), before chemical etching in HF (HF:H_2O = 0.02:1 (48% HF), 40 s) selectively etches the SiO_2 layers to form individual lamellae ledges approximately 30 nm in depth (Figure 3a,iii). Silver nanoparticles are removed (HNO_3:H_2O = 0.1:1 (70% HNO_3), 38 min) (Figure S9) to reveal large-area self-assembled Bragg butterfly nanostructures (Figure 3b). These nanostructures are fabricated without the use of lithography, nanoimprinting, or other common cleanroom nanofabrication techniques, but instead by inherently scalable self-assembly.

UV−vis reflection and transmission spectra were measured using a spectrometer with an integrating sphere (PerkinElmer), demonstrating a characteristic Bragg long-pass filter response centered at 600 nm with strong reflection about λ_0 and high transmission beyond ∼650 nm (Figure 4a).

Angular-resolved reflectance spectra were also collected for wavelengths of 400−820 nm using the same spectrometer with an ARTA attachment, with a detector height of 7 mm, a width of 32 mm, and a distance of 120 mm from the sample (Figure 4b). Integrating the scattered reflectance in the solid angle, we find more than half of all reflected light below the cutoff wavelength of the Bragg filter is scattered into angles of >10°, providing the first demonstration of a short-wavelength scattering long-pass filter fabricated via large-area self-assembly. More than 95% of transmitted light is forward scattered at angles of <5° from normal (Figure S8b). The broadband absorption observed in Figure 4a is caused by silicon-rich SiON layers[34] and can be mitigated through the replacement of SiON with a less absorbing high-refractive index material such as TiO_2. The strong nonspecular reflection is expected to be further enhanced through (i) a deeper HF etch of the lamellae,
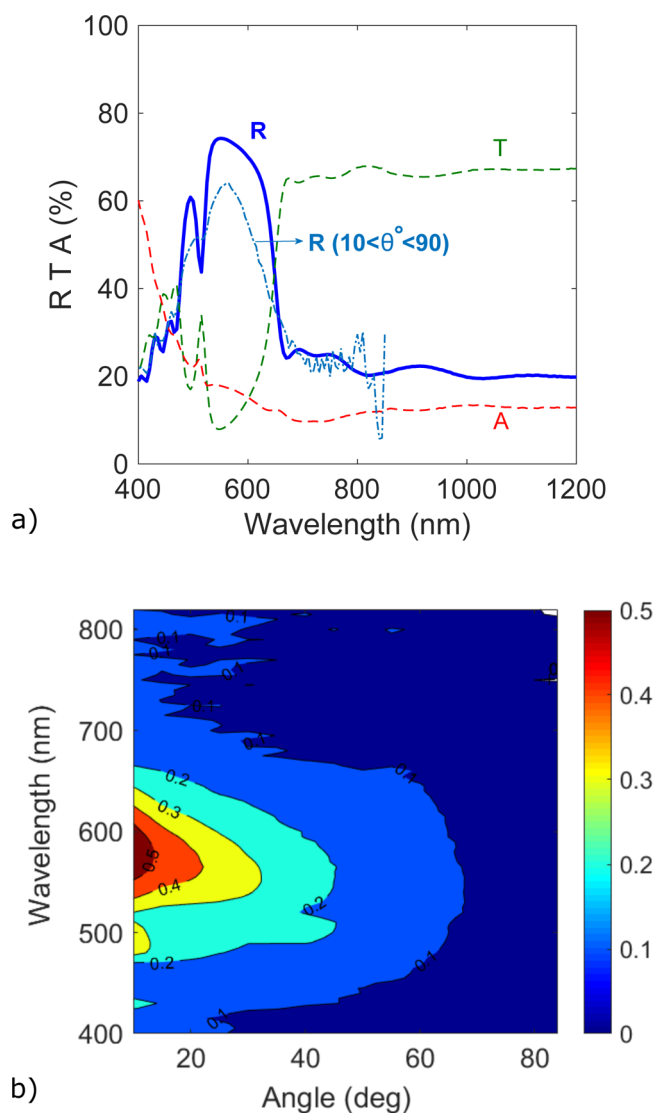
a)

b)

Figure 4. (a) Reflection, transmission, and absorption of large-area transparent scatterer, obtained via an integrating sphere. Dashed line: integrated nonspecular reflection (10° < θ < 90°). (b) Angularly resolved reflectance.

(ii) use of materials with higher refractive-index contrast, (iii) taller nanostructures, and (iv) use of materials with less optical absorption.

We demonstrate long-pass transmission with short-wavelength scattering for visible light, but expect the principle to be widely applicable across the electromagnetic spectrum. Our initial motivation was for light trapping in tandem solar cells,[10] but we identify here the possibilities for a wide range of future nuanced applications for the transmission and scattering of light including those as varied as scalable anticounterfeiting,[5] optical camouflage while allowing long-wavelength communication,[3] batch signals processing,[6] and architectural windows with a matte blue exterior allowing red-light transmission.[4,40]

■ CONCLUSION

By combining the optical principles of moth-eye antireflection, Bragg scattering, and planar long-pass dielectric filters, we are able to design and fabricate a short-wavelength scattering/long-pass filter with sharp cutoff, high transmission of infrared light, and strong reflection of visible light into high angles. Based on

the lamellae-edge features on *M. didius* butterfly wings, nanostructures are self-assembled via sequential one-chamber chemical vapor deposition, metal nanoparticle formation, and wet-chemical etching.

Finite-element modeling demonstrates strong (>45%) reflection into the first diffracted order for short wavelengths, while retaining >80% transmission for longer wavelengths. Fabricated nanostructures couple more than 50% of reflected light into angles of >10° while enabling broadband long-pass transmission. While these principles are demonstrated in the visible regime, they are expected to be widely applicable across the electromagnetic spectrum. Such structures have potential applications in light trapping for tandem solar cells, stealth, architecture, and signals processing.

■ ASSOCIATED CONTENT

ⓢ Supporting Information

The Supporting Information is available free of charge on the ACS Publications website at DOI: 10.1021/acsphotonics.6b01007.

Complete modeling results for varying periods, modeling results for SiON structures, measured reflection spectra for five batch samples, measured angular transmittance spectra, additional details of optical measurement and nanostructure fabrication, and additional scanning electron micrographs (PDF)

■ AUTHOR INFORMATION

Corresponding Author

*E-mail: niraj.lal@anu.edu.au.

ORCID ⓘ

Niraj N. Lal: 0000-0002-2393-176X

Notes

The authors declare no competing financial interest.

■ REFERENCES

(1) Boriskina, S. V.; Green, M. A.; Catchpole, K.; Yablonovitch, E.; Beard, M. C.; Okada, Y.; Lany, S.; Gershon, T.; Zakutayev, A.; Tahersima, M. H.; Sorger, V. J.; Naughton, M. J.; Kempa, K.; Dagenais, M.; Yao, Y.; Xu, L.; Sheng, X.; Bronstein, N. D.; Rogers, J. A.; Alivisatos, A. P.; Nuzzo, R. G.; Gordon, J. M.; Wu, D. M.; Wisser, M. D.; Salleo, A.; Dionne, J.; Bermel, P.; Greffet, J.-J.; Celanovic, I.; Soljacic, M.; Manor, A.; Rotschild, C.; Raman, A.; Zhu, L.; Fan, S.; Chen, G. Roadmap on Optical Energy Conversion. *J. Opt.* **2016**, *18*, 73004.

(2) Pelka, D. G.; Patel, K. An Overview of LED Applications for General Illumination. *Proc. SPIE* **2003**, 55.

(3) Lynch, D. *Introduction to RF Stealth*; SPIE Press, 2004.

(4) Arbab, M.; Finley, J. J. Glass in Architecture. *Int. J. Appl. Glass Sci.* **2010**, *1*, 118.

(5) Phillip, R. W.; Bleikolm, A. F. Optical Coatings for Document Security. *Appl. Opt.* **1996**, *35*, 5529.

(6) Yu, F. T. S.; Jutamulia, S. *Optical Signal Processing, Computing, and Neural Networks*; Wiley, 1992.

(7) Oldenburg, S.; Averitt, R.; Westcott, S.; Halas, N. Nano-engineering of Optical Resonances. *Chem. Phys. Lett.* **1998**, *288*, 243.

(8) Green, M. A. Lambertian Light Trapping in Textured Solar Cells and Light-Emitting Diodes: Analytical Solutions. *Prog. Photovoltaics* **2002**, *10*, 235.

(9) Zeng, L.; Bermel, P.; Yi, Y.; Alamariu, B. A.; Broderick, K. A.; Liu, J.; Hong, C.; Duan, X.; Joannopoulos, J.; Kimerling, L. C. Demonstration of Enhanced Absorption in Thin Film Si Solar Cells with Textured Photonic Crystal Back Reflector. *Appl. Phys. Lett.* **2008**, *93*, 221105.

(10) Lal, N. N.; White, T. P.; Catchpole, K. R. Optics and Light Trapping for Tandem Solar Cells on Silicon. *IEEE J. Photovoltaics* **2014**, *4*, 1380.

(11) Vukusic, P.; Sambles, J. R. Photonic Structures in Biology. *Nature* **2003**, *424*, 852.

(12) Vukusic, P.; Hallam, B.; Noyes, J. Brilliant Whiteness in Ultrathin Beetle Scales. *Science* **2007**, *315*, 348.

(13) Parker, A. R.; et al. 515 Million Years of Structural Colour. *J. Opt. A: Pure Appl. Opt.* **2000**, *2*, R15.

(14) Vignolini, S.; Rudall, P. J.; Rowland, A. V.; Reed, A.; Moyroud, E.; Faden, R. B.; Baumberg, J. J.; Glover, B. J.; Steiner, U. Pointillist Structural Color in Pollia Fruit. *Proc. Natl. Acad. Sci. U. S. A.* **2012**, *109*, 15712.

(15) Kinoshita, S.; Yoshioka, S.; Kawagoe, K. Mechanisms of Structural Colour in the Morpho Butterfly: Cooperation of Regularity and Irregularity in an Iridescent Scale. *Proc. R. Soc. London, Ser. B* **2002**, *269*, 1417.

(16) Aryal, M.; Ko, D. H.; Tumbleston, J. R.; Gadisa, A.; Samulski, E. T.; Lopez, R. Large Area Nanofabrication of Butterfly Wing's Three Dimensional Ultrastructures. *J. Vac. Sci. Technol., B: Nanotechnol. Microelectron.: Mater., Process., Meas., Phenom.* **2012**, *30*, 61802.

(17) Pris, A. D.; Utturkar, Y.; Surman, C.; Morris, W. G.; Vert, A.; Zalyubovskiy, S.; Deng, T.; Ghiradella, H. T.; Potyrailo, R. A. Towards High-Speed Imaging of Infrared Photons with Bio-Inspired Nano-architectures. *Nat. Photonics* **2012**, *6*, 195.

(18) Hecht, E. *Optics*, 4th ed.; Addison Wesley: San Francisco, 2002.

(19) Orfanidis, S. *Electromagnetic Waves and Antennas*; Rutgers University: NJ, 2002.

(20) De Wolf, S.; Holovsky, J.; Moon, S.-J.; Löper, P.; Niesen, B.; Ledinsky, M.; Haug, F.-J.; Yum, J.-H.; Ballif, C. Organometallic Halide Perovskites: Sharp Optical Absorption Edge and Its Relation to Photovoltaic Performance. *J. Phys. Chem. Lett.* **2014**, *5*, 1035.

(21) Loper, P.; Niesen, B.; Moon, S.-J.; Martin de Nicolas, S.; Holovsky, J.; Remes, Z.; Ledinsky, M.; Haug, F.-J.; Yum, J.-H.; De Wolf, S.; Ballif, C. Organic-Inorganic Halide Perovskites: Perspectives for Silicon-Based Tandem Solar Cells. *IEEE J. Photovoltaics* **2014**, *4*, 1545.

(22) Hoffmann, A.; Paetzold, U. W.; Zhang, C.; Merdzhanova, T.; Lambertz, A.; Ulbrich, C.; Bittkau, K.; Rau, U. Advancing Tandem Solar Cells by Spectrally Selective Multilayer Intermediate Reflectors. *Opt. Express* **2014**, *22*, A1270.

(23) Bielawny, A.; Rockstuhl, C.; Lederer, F.; Wehrspohn, R. B. Intermediate Reflectors for Enhanced Top Cell Performance in Photovoltaic Thin-Film Tandem Cells. *Opt. Express* **2009**, *17*, 8439.

(24) Üpping, J.; Bielawny, A.; Wehrspohn, R. B.; Beckers, T.; Carius, R.; Rau, U.; Fahr, S.; Rockstuhl, C.; Lederer, F.; Kroll, M.; Pertsch, T.; Steidl, L.; Zentel, R. Three-Dimensional Photonic Crystal Inter-mediate Reflectors for Enhanced Light-Trapping in Tandem Solar Cells. *Adv. Mater.* **2011**, *23*, 3896.

(25) Wehrspohn, R. B.; Üpping, J. 3D Photonic Crystals for Photon Management in Solar Cells. *J. Opt.* **2012**, *14*, 24003.

(26) Wilson, S.; Hutley, M. The Optics of "Moth Eye" Antireflection Surfaces. *Opt. Acta* **1982**, *29*, 7.

(27) Sun, C.-H.; Jiang, P.; Jiang, B. Broadband Moth-Eye Antireflection Coatings on Silicon. *Appl. Phys. Lett.* **2008**, *92*, 61112.

(28) Boden, S. A.; Bagnall, D. M. Tunable Reflection Minima of Nanostructured Antireflective Surfaces. *Appl. Phys. Lett.* **2008**, *93*, 133108.

(29) Vukusic, P.; Sambles, J. R.; Lawrence, C. R.; Wootton, R. J. Quantified Interference and Diffraction in Single Morpho Butterfly Scales. *Proc. R. Soc. London, Ser. B* **1999**, *266*, 1403.

(30) Potyrailo, R. A.; Starkey, T. A.; Vukusic, P.; Ghiradella, H.; Vasudev, M.; Bunning, T. Discovery of the Surface Polarity Gradient on Iridescent Morpho Butter Fly Scales Reveals a Mechanism of Their Selective Vapor Response. *Proc. Natl. Acad. Sci. U. S. A.* **2013**, *110*, 15567.

(31) Siddique, R. H.; Diewald, S.; Leuthold, J.; Hendrik, H. *Opt. Express* **2013**, *21*, 14351.

(32) Malitson, I. H. Interspecimen Comparison of the Refractive Index of Fused Silica*,†. *J. Opt. Soc. Am.* **1965**, *55*, 1205.

(33) DeVore, J. R. Refractive Indices of Rutile and Sphalerite. *J. Opt. Soc. Am.* **1951**, *41*, 416.

(34) Thomson, A.; Lal, N.; Wan, Y. Interpolating the Optical Properties of Varied Composition Silicon Nitride. *Phys. Status Solidi B* **2015**, *252*, 2230.

(35) Prum, R. O.; Torres, R; Williamson, S.; Dyck, J. Two-Dimensional Fourier Analysis of the Spongy Medullary Keratin of Structurally Coloured Feather Barbs. *Proc. R. Soc. London, Ser. B* **1999**, *266*, 1414.

(36) Prum, R. O.; Torres, R. H.; Williamson, S.; Dyck, J. Coherent Light Scattering by Blue Feather Barbs. *Nature* **1998**, *396*, 28.

(37) Scarmozzino, R.; Gopinath, A.; Pregla, R.; Helfert, S. Numerical Techniques for Modeling Guided-Wave Photonic Devices. *IEEE J. Sel. Top. Quantum Electron.* **2000**, *6*, 150.

(38) Bienstman, P.; Baets, R. Optical Modelling of Photonic Crystals and VCSELs Using Eigenmode Expansion and Perfectly Matched Layers. *Opt. Quantum Electron.* **2001**, *33*, 327.

(39) Lecamp, G.; Hugonin, J. P.; Lalanne, P. Theoretical and Computational Concepts for Periodic Optical Waveguides. *Opt. Express* **2007**, *15*, 11042.

(40) Mohelnikova, J. Materials for Reflective Coatings of Window Glass Applications. *Constr. Build. Mater.* **2009**, *23*, 1993.

(41) Descouens, D. Morpho Menelaus Didius Butterfly. *Wikimedia Commons* **2011**.